J. Fluid Mech. (1987), *vol.* 177, *pp.* 167–186
Printed in Great Britain

Surface pressure fluctuations in a separating turbulent boundary layer

By ROGER L. SIMPSON†, M. GHODBANE AND B. E. McGRATH†
Southern Methodist University, Dallas, TX 75275, USA

(Received 21 February 1986 and in revised form 30 June 1986)

Measurements of surface pressure-fluctuation spectra and wave speeds are reported for a well-documented separating turbulent boundary layer. Two sensitive instrumentation microphones were used in a new technique to measure pressure fluctuations through pinhole apertures in the flow surface. Because a portion of the acoustic pressure fluctuations is the same across the nominally two-dimensional turbulent flow, it is possible to decompose the two microphone signals and obtain the turbulent flow contributions to the surface pressure spectra. In addition, data from several earlier attached-flow surface-pressure-fluctuation studies are re-examined and compared with the present measurements.

The r.m.s. of the surface pressure fluctuation p' increases monotonically through the adverse-pressure-gradient attached-flow region and the detached-flow zone. Apparently p' is proportional to the ratio α of streamwise lengthscale to lengthscales in other directions. For non-equilibrium separating turbulent boundary layers, α is as much as 2.5, causing p' to be higher than equilibrium layers with lower values of α.

The maximum turbulent shearing stress τ_M appears to be the proper stress on which to scale p'; p'/τ_M from available data shows much less variation than when p' is scaled on the wall shear stress. In the present measurements p'/τ_M increases to the detachment location and decreases downstream. This decrease is apparently due to the rapid movement of the pressure-fluctuation-producing motions away from the wall after the beginning of intermittent backflow. A correlation of the detached-flow data is given that is derived from velocity- and lengthscales of the separated flow.

Spectra $\Phi(\omega)$ for $\omega\delta^*/U_\infty > 0.001$ are presented and correlate well when normalized on the maximum shearing stress τ_M. At lower frequencies, for the attached flow $\Phi(\omega) \sim \omega^{-0.7}$ while $\Phi(\omega) \sim \omega^{-3}$ at higher frequencies in the strong adverse-pressure-gradient region. After the beginning of intermittent backflow, $\Phi(\omega)$ varies with ω at low frequencies and ω^{-3} at high frequencies; farther downstream the lower-frequency range varies with $\omega^{1.4}$.

The celerity of the surface pressure fluctuations for the attached flow increases with frequency to a maximum; at higher frequencies it decreases and agrees with the semi-logarithmic overlap equation of Panton & Linebarger. After the beginning of the separation process, the wave speed decreases because of the oscillation of the instantaneous wave speed direction. The streamwise coherence decreases drastically after the beginning of flow reversal.

† Present address: Department of Aerospace and Ocean Engineering, Virginia Polytechnic Institute and State University, Blacksburg, VA 24061, USA.

1. Introduction

Noise generated by helicopter and turbomachine rotors is a nuisance that designers would like to predict and to minimize within other design constraints. Brooks & Schlinker (1983) reviewed some recent research on helicopter rotor noise and discussed the categories of noise sources, which include blade self-noise generation by strong adverse-pressure-gradient attached turbulent boundary layers and by separated turbulent boundary layers that accompany stall.

Brooks & Hodgson (1981) showed that starting with given surface pressure-fluctuation spectra and convective speeds, radiated noise due to the turbulent boundary layer can be predicted. Furthermore, if the surface pressure-fluctuation spectra and convective speeds can be related to the turbulent flow structure, then turbulent-boundary-layer flow field calculation methods can be used when designing rotors to estimate the required surface pressure-fluctuation information.

Thus, a key requirement for this noise calculation procedure is knowledge relating the flow field structure to the surface-pressure-fluctuation structure. Unfortunately there are few measurements of both flow-field structure and surface-pressure-fluctuation structure for a given flow, especially in the presence of adverse pressure gradients and separation. Detailed flow-field measurements have been made of a nominally two-dimensional, steady free stream, separated turbulent boundary layer (Simpson, Shivaprasad & Chew 1981). This article presents information on the surface pressure fluctuations for this well-documented velocity flow field. To our knowledge there are no other measurements available of these properties for such a separating turbulent boundary layer.

Some previous work on surface pressure fluctuations for zero and adverse-pressure-gradient and step-induced separating turbulent boundary layer flows is discussed and the data reanalysed in the next section. A summary of the nature of this separating turbulent-boundary-layer flow field is given. In following sections the experimental instrumentation, techniques and results are discussed for the surface pressure-fluctuation spectra and celerities.

2. Re-examination of some previous work on surface pressure fluctuations

First, it should be stated that local static pressure fluctuations can only be measured non-intrusively at the wall in a turbulent boundary layer. Small sensing surfaces must be used to detect fluctuations that are larger in spatial scale. Small pinhole openings in the surface have been used to measure fluctuations with sensitive microphones. Small less-sensitive piezoelectric transducers flush with the surface have also been used to avoid any influence of a pinhole on the flow. Flow disturbances are present in most wind tunnels, so measurements of the low-frequency components of the wall pressure fluctuations are impossible to make with a single sensor. Willmarth (1975) reviewed many measurements, pointing out the shortcomings of each set of available data. Needless to say, there are significant differences between results obtained for approximately the same flow conditions by different investigators.

As in all practical turbulent-flow problems, purely theoretical calculations of surface pressure fluctuations have not yet been done successfully. In incompressible turbulent flow the fluctuating pressure p is related to the velocity fluctuations by the Poisson equation

$$\frac{\partial^2 p}{\partial x_1^2} = -\rho\sigma, \tag{1}$$

where the source term σ is given in tensor notation by

$$\sigma = 2\frac{\partial U_i}{\partial x_j}\frac{\partial u_j}{\partial x_i} + \frac{\partial^2}{\partial x_i \partial x_j}(u_i u_j - \overline{u_i u_j}), \tag{2}$$

and U_i and u_i are the mean and fluctuating velocity components in the x_i direction. The first term on the right-hand side of this equation represents the turbulence and mean-shear interaction while the second term represents the turbulence–turbulence interaction. For a wall-bounded flow, if contributions from surface integrals are neglected, then the fluctuating pressure at a point $\boldsymbol{X}$ on the wall is given by

$$p(\boldsymbol{X}) = \frac{\rho}{2\pi}\int_{Y>0} \frac{\sigma(\boldsymbol{R}_s)\,\mathrm{d}V(\boldsymbol{R}_s)}{(\boldsymbol{X}-\boldsymbol{R}_s)}, \tag{3}$$

where the volume V integration is at position $\boldsymbol{R}_s$ over the entire half-space containing the flow. This equation indicates that while surface pressure fluctuations are produced from sources in a large region of the flow, contributions from various sources drop off rapidly with their distance from the point under consideration. Although several attempts have been made to calculate p from (3), Willmarth (1975) pointed out that it appears that such efforts suffer from the lack of accurate information about the fluctuating velocity field within the boundary layer. Consequently, the effects of adverse pressure gradients and separation on surface pressure fluctuations from such calculations are uncertain and need confirmation by experimental data.

Panton & Linebarger (1974) calculated wall pressure spectra for zero-pressure-gradient and adverse-pressure-gradient equilibrium boundary layers that seem to describe the essential features observed from experiments. They used Coles' laws of the wall and wake for the mean velocity profiles. A scale-anisotropic model of the spatial correlation of v was used together with the assumption that v was proportional to $(-\overline{uv})^{\frac{1}{2}}$. As in some earlier calculations, only the turbulence and mean-shear interaction was modelled since the turbulence–turbulence interaction contributes only a very small portion to the mean-square value.

Their spectral results showed larger contributions at higher Reynolds numbers for $(2\pi/\lambda)\,\delta = k\delta < 20$. The contributions to the spectrum at these low frequencies and wavenumbers k are due to the outer-region velocity and turbulence structure and depend upon the pressure gradient. An overlap region between the low-frequency outer-region contributions and the high-frequency near-wall viscous-dominated part of the wavenumber spectrum $F(k)$ varies with k^{-1}, as shown by Bradshaw (1967) using dimensional analysis. For this overlap region, we can approximate their calculation results by

$$\frac{kF(k)}{\tau_w^2} \approx 1.73\alpha^{0.9} \quad \text{for } \frac{k\nu}{U_\tau} < 0.06, \tag{4}$$

which closely agrees with the zero-pressure-gradient measurements of McGrath & Simpson (1985). Here α is the ratio of the streamwise lengthscale to lengthscales in other directions, which strongly influences the spatial correlation of v. At higher frequencies, their spectra decay rapidly and scale also on the wall shearing stress τ_w and shear velocity $U_\tau = (\tau_w/\rho)^{\frac{1}{2}}$.

Because the low-frequency part of the spectrum is Reynolds-number dependent, the mean-square pressure fluctuation increases with boundary-layer-thickness Reynolds number. Here we present an equation,

$$\frac{\overline{p^2}}{\tau_w^2} = 0.52\alpha^{0.9}\left(\ln\left|\frac{U_\tau\delta}{\nu}\right| + 9.24\right), \tag{5}$$

that fits Panton & Linebarger's calculations for a zero pressure gradient with $\alpha = 1$, 2 and 3, and a Coles' wake-function parameter $\pi = 0.6$. In terms of the displacement-thickness Reynolds number

$$\frac{U_\tau \delta}{\nu} = \frac{K}{1+\pi}\left(\frac{U_\infty \delta^*}{\nu} - 65\right), \tag{6}$$

where $K = 0.41$ (Coles & Hirst 1969).

Bull & Thomas (1976) suggest that spectral measurements with a pinhole microphone of zero-pressure-gradient flow, such as Blake's (1970), are too high for frequencies $n(\omega = 2\pi n)$ higher than the high-frequency end of the overlap region, $\omega\nu/U_\tau^2 > 0.1$. This apparent pinhole effect extends to $\omega\nu/U_\tau^2 > 2$. The pinhole microphone interacts with the viscous flow to amplify the frequencies in this range. The spurious amplification appears to be a function of $\omega\nu/U_\tau^2$ for the narrow range of test parameters that were used. Bull (1967), Lim (1971) and Schloemer (1967) used flush-surface piezoelectric pressure transducers that were relatively large, so high-frequency contributions to the mean-square pressure fluctuation were attenuated (Willmarth 1975). Consequently, the r.m.s. pressure fluctuations for these latter measurements were 30%, 20% and 40% lower than (5), respectively.

The spectral measurements of Bull & Thomas (1976) show a short $\Phi(\omega) \sim \omega^{-1}$ region $(0.05 < \omega\nu/U_\tau^2 < 0.2)$ and a higher frequency $\Phi(\omega) \sim \omega^{-3}$ region $(\omega\nu/U_\tau^2 > 0.5)$. Here $\overline{p^2} = 2\int_0^\infty \phi(\omega)\,\mathrm{d}\omega$. Their pressure-fluctuation measurements with a piezoelectric transducer are 4% lower than (5) because the sensing diameter was too large $(44 < dU_\tau/\nu < 65)$ to pick up the smallest wavelength λ_z near-wall turbulent motions $(\lambda_z U_\tau/\nu \approx 12)$ (Simpson 1976).

At the lower frequencies of the overlap region, the pressure-fluctuation spectrum for the zero-pressure-gradient case scales approximately on the outer variables, free-stream dynamic pressure q_∞, U_∞ and δ^*. The spectral level seems to be almost the same in various investigations, with

$$10\log_{10}\left|\frac{\Phi(\omega)\,U_\infty}{q_\infty^2\,\delta^*}\right| = -51 \pm 2 \quad \text{at} \quad \frac{\omega\delta^*}{U_\infty} = 1 \tag{7}$$

(Bull & Thomas 1976; Burton 1973; Willmarth 1975; Schloemer 1967; Panton & Linebarger 1974). For $0.1 < \omega\delta^*/U_\infty < 1$, $\Phi(\omega)$ levels off and is approximately constant in most investigations. For the lowest measurable frequencies, $\Phi(\omega)$ generally increases slightly with ω, although there is some scatter in data due to different low-frequency disturbances in different test wind tunnels.

For adverse-pressure-gradient equilibrium turbulent boundary layers, the low frequency part of the spectrum $(k\delta < 20)$ should scale approximately on the local maximum shearing stress τ_M in the boundary layer (Mabey 1982). The calculated low-frequency spectra shown in figure 10 of Panton & Linebarger (1974) for $\pi = 1.5$, 3 and 6 collapse together when rescaled on τ_M. Here we have estimated the maximum shearing stress from the shape factor H and

$$\frac{\tau_M}{\rho U_\infty^2} = \left[\frac{1}{6.55}\left(1 - \frac{1}{H}\right)\right]^2 \tag{8}$$

(East & Sawyer 1979). Table 1 shows that $\overline{p^2}/\tau_M^2$ from Panton & Linebarger is nearly constant while $\overline{p^2}/\tau_w^2$ varies over an order of magnitude. This scaling on τ_M is supported by (3) and the structure of strong adverse-pressure-gradient and separating turbulent boundary layers, as discussed below.

Authors	$Re_{\delta^*} 10^{-3}$	$\frac{U_\tau}{U_\infty}$	π	H	$\frac{U_M}{U_\infty}$	$\frac{dU_\tau}{\nu}$	$\frac{\overline{p^2}}{\tau_w^2}$	$\frac{\overline{p^2}}{\tau_M^2}$	$\Phi(\omega_1) \sim \omega_1^{-1}$ region	$\Phi(\omega_1) \sim \omega_1^{-3}$ region	Comments
Panton & Linebarger (1974)	9.8	0.0307	1.5	1.49	0.0504†	—	19.1	2.62	NA	NA	$\alpha = 1$
	39.1	0.0251	3	1.627	0.0589†	—	62.4	2.06	$\omega_1 \approx 0.6$	$1 < \omega_1 < 3$	$\alpha = 1$
calculations;	39.1	0.0251	3	1.627	0.0589†	—	130	4.29	$\omega_1 \approx 0.4$	$1 < \omega_1 < 3$	$\alpha = 2$
equilibrium	68.3	0.0183	6	1.824	0.0690†	—	395	1.96	NA	NA	$\alpha = 1$
Bradshaw (1967) equilibrium	40.3	0.0252	2.9	1.59	0.0566	191	78	3.4	$\omega_1 \approx 0.6$	$3 < \omega_1 < 6$	piezoelectric transducer; $X = 1.22$ m
Lim (1971) equilibrium	28.4	0.0291	1.92†	1.56	0.0546†	53.8	16.8	1.52	$0.8 < \omega_1 < 2$	not observed	$X = 2.9$ m; piezoelectric transducers
	32.4	0.0294	1.92†	1.52	0.0519†	59.2	18.8	1.73	$0.8 < \omega_1 < 2$	not observed	$X = 3.2$ m; no turbulence measurements
Schloemer (1967) non-equilibrium	14.6	0.0296	1.84†	1.58	0.0563†	126	18.9	1.44	$0.8 < \omega_1 < 1$	$\omega_1 > 6$	piezoelectric
Burton (1973) non-equilibrium	NA	0.023	NA	1.76	0.059	≈ 38	92	2.12	$\omega_1 \approx 0.4$	$\omega_1 > 2$	$X/\delta^* = 14.5$; pinhole microphone
	38	0.021	4.7†	2.23	0.060		131	1.97	$\omega_1 \approx 0.4$	$\omega_1 > 2$	$X/\delta^* = 24.3$
Hahn (1976) airfoil	48	0.030	0.9†	1.33	0.038	274	19.6	7.5	$0.5 < \omega_1 < 10$	NA	piezoelectric transducers
Brooks & Hodgson (1981) airfoil	19	0.032	NA	1.5	0.051†	40	NA	NA	$0.5 < \omega_1 < 5$	NA	piezoelectric transducers

TABLE 1. Some pressure-fluctuation results from adverse-pressure-gradient turbulent boundary layers, $\omega_1 = \omega\delta^*/U_\infty$; † denotes values estimated from equilibrium boundary-layer equations for the laws of wall and wake or equation (8); NA denotes data not available

Perry & Schofield (1973) proposed universal empirical correlations for the inner and outer mean-velocity-profile regions of strong adverse-pressure-gradient boundary layers near separation, including both equilibrium and non-equilibrium profiles. The data of Simpson, Strickland & Barr (1977) and Simpson *et al.* (1981) upstream of any flow reversal agree with these correlations. The Reynolds-shearing-stress profile and the maximum shearing stress τ_M (which occurs in the middle of the boundary layer) play important roles in these correlations when $\tau_M > 1.5\tau_w$. In other words, the same large-scale turbulent structures that produce the maximum shearing stress away from the wall are the structures that influence the mean velocity profile from near the wall to the outer edge.

Perry & Schofield proposed that the outer-region flow be described by

$$\frac{U_\infty - U}{U_s} = f_2\left(\frac{y}{\Delta}\right), \quad \Delta = 2.86\frac{\delta^* U_\infty}{U_s}, \tag{9}$$

with

$$U_s \approx 8U_M\left(\frac{\Delta}{N}\right)^{\frac{1}{2}}, \quad U_M = \left(\frac{\tau_M}{\rho}\right)^{\frac{1}{2}}, \tag{10}$$

N being the distance from the wall to the maximum in the local shear-stress profile.

Thus using (3), (9) and (10) and scaling the turbulence structure on τ_M and Δ, we propose here that

$$p \sim \rho U_s U_M \tag{110}$$

or that

$$p \sim \tau_M\left(\frac{\Delta}{N}\right)^{\frac{1}{2}} \sim \tau_M\left(\frac{\delta^* U_\infty}{N U_M}\right)^{\frac{1}{2}}. \tag{12}$$

Table 1 shows that $\overline{p^2}/\tau_M^2$ values from experiments are in approximate agreement with Panton & Linebarger's calculations. It appears that $\overline{p^2}/\tau_M^2$ decreases with increasing H, although there are insufficient data to be sure of this and the Δ/N dependence given in (12). When $\tau_M/\tau_w < 1.5$, we would expect $\overline{p^2}/\tau_M^2$ to approach 9, which is the order of the zero-pressure-gradient value. Hahn's (1976) data support this observation. The effect of transducer size on these data is not clear since $\overline{p^2}/\tau_M^2$ does not consistently decrease with increasing dU_τ/ν.

Figure 1 shows spectra, corrected for transducer size by their originators, that correspond to the strong adverse-pressure-gradient data of table 1 when re-normalized here on τ_M. The data of Schloemer (1967), Bradshaw (1967), Burton (1973) and Lim (1971) for $H < 2$ and the calculations of Panton & Linebarger (1974) for $\alpha = 1$ agree to within a few dB for $\omega\delta^*/U_\infty < 5$. All results seem to agree at $\omega\delta^*/U_\infty = 1$. At higher $\omega\delta^*/U_\infty$ values, Lim's data are much higher than those of the others; Panton & Linebarger's calculations appear to be higher. As shown in table 1, the ω^{-1} region becomes narrower at higher H-values until it is only a point near $\omega\delta^*/U_\infty = 0.5$. A ω^{-3} region at higher frequencies is observed for the higher H-values.

The $\alpha = 2$ calculations of Panton & Linebarger agree fairly well with Burton's spectral data for $H = 2.23$. These calculations suggest that the ratios of streamwise lengthscale to lengthscales in other directions are greater than one for strongly retarded boundary layers. The spatial correlation data of Schubauer & Klebanoff (1951) for a strongly retarded separating turbulent boundary layer indicate that the streamwise integral lengthscale is about 2.5 times the normal-to-wall integral lengthscale. The calculations of Panton & Linebarger suggest that $\overline{p^2}/\tau_M^2 \sim \alpha$. The spectrum above $\omega\delta_1/U_\infty = 1$ does not appear to be influenced by α, either in calculations or in the data. Thus, the low-frequency part of the spectrum for strongly retarded adverse-pressure-gradient boundary layers appears to be large because α is much greater than one.

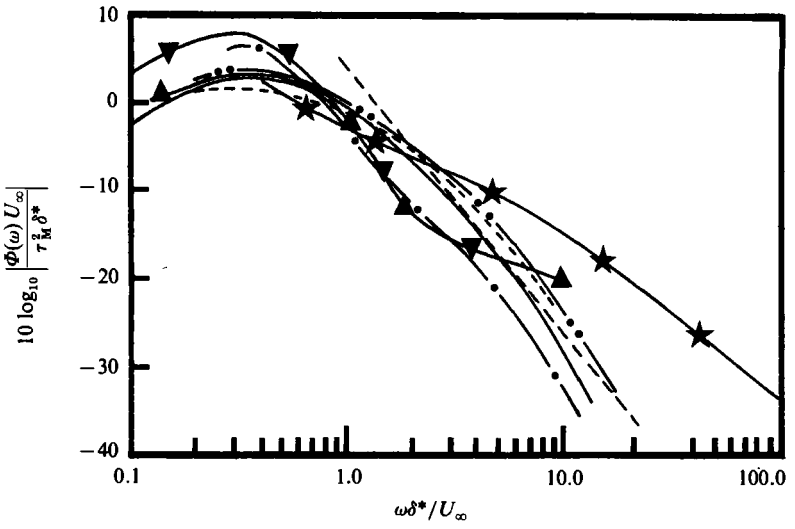

FIGURE 1. Spectra from some strong adverse-pressure-gradient turbulent boundary layers. Straight dashed line: ω^{-1} variation. ----, Schloemer (1967) $Re_{\delta^*} \times 10^{-4} = 1.46$; ——, Bradshaw (1967) $Re_{\delta^*} \times 10^{-4} = 4.0$; -●-, Burton (1973) $Re_{\delta^*} \times 10^{-4} = 3.8$; -●●-, Burton (1973) $Re_{\delta^*} \times 10^{-4} = 2.4$; -★-, Lim (1971) $Re_{\delta^*} \times 10^{-4} = 3.2$; -▲-, Panton & Linebarger (1974) $Re_{\delta^*} \times 10^{-4} = 4.0$, $\alpha = 1$; -▼-, Panton & Linebarger (1974) $Re_{\delta^*} \times 10^{-4} = 4.0$, $\alpha = 2$.

Panton & Linebarger proposed that the convective velocity $U_c(k)$ for the overlap region of the k^{-1} part of the spectrum for an attached boundary layer can be described by

$$\frac{U_c}{U_\tau} = \frac{1}{K}\ln\left|\frac{u_\tau}{k\nu}\right| + 5.0. \tag{13}$$

This expression is the same as the semi-logarithmic mean-velocity-profile equation, with $U_c = U$ at $y = 1/k$. They showed that this expression agrees very well with the data of Bradshaw (1967) and Wills (1970) for $6 < k\delta < 40$ or the k^{-1} part of the spectrum. This expression also fits the measured U_c/U_∞ data of Schloemer to within 10% for adverse, zero, and favourable pressure gradients in the k^{-1} part of the spectrum. The adverse-pressure-gradient data of Burton (1973), Brooks & Hodgson (1981) and Hahn (1976) for the closest sensor spacings also are described to within 15% by this equation in the overlap region.

These latter sets of data, obtained using space–time correlations or cross-spectral phase information, show that the apparent $U_c(k)$ increases with increasing sensor spacing because the coherence of smaller-scale turbulent motions at a given frequency decays more. Schloemer found that the decay of a particular frequency component with respect to distance was more rapid in an adverse gradient and slower in a favourable gradient than the decay in a zero pressure gradient. This amounts to spatial filtering of the eddies, causing the more coherent faster large-scale structures to contribute more to the apparent U_c at increasing spacings. Bradshaw (1967) pointed out that the average convection velocity at a given wavenumber k is the average over all frequencies in the (k, ω)-plane. Like Wills, Bradshaw took the one-dimensional Fourier transform of frequency-filtered spatial correlations to obtain $U_c(k, \omega)$. This approach produces the complete distribution of U_c at all k, while spatial-filtering approaches produce large-eddy weighted averages.

The convective velocity reaches a peak value at a frequency near the lower end of the overlap part of the spectrum. Bradshaw's data show this peak near

$\omega\delta^*/U_\infty = 0.5$, while Brooks & Hodgson show a peak near $\omega\delta^*/U_\infty = 3.0$. Brooks & Hodgson, Wills and Bradshaw show that U_c decreases below this peak. Schloemer and Burton do not have data for this low-frequency range while Hahn's results show numerous U_c maxima and minima. Panton & Linebarger suggested an approximate wake-function expression for this low-frequency range.

Mabey (1972) presented a correlation of r.m.s. pressure fluctuations and spectra for step-induced separation and reattachment flows. The length of the detached-flow zone S is a good normalizing length that causes the shapes of the plots to be similar. In p'/q *vs.* X/S plots, p' increases rapidly after detachment, reaching an order-of-magnitude greater maximum just upstream of reattachment. At this maximum, p'/q_∞ varied from 0.04 to 0.1, depending on the type of detached flow. In $\omega\Phi(\omega)$ *vs.* $\omega S/U_\infty$ spectral plots, the peak frequency is located just below a $\omega S/U$ of 2π. Since no data for the Reynolds shear stress $-\rho\overline{uv}$ profiles are available, it is not possible to correlate further these data.

Kiya, Sasaki & Arie (1982) showed similar results for a forward-facing step flow: p'/q_∞ reached a maximum of 0.14 at $X/L = 1$; $\omega\Phi(\omega)$ reaches a maximum at $\omega S/U_\infty \approx 1.4\pi$ and decays proportional to ω^{-2} at higher frequencies. Near reattachment, $p'/\tau_M = 10$, which is an order-of-magnitude greater than the values given in table 1 for attached flows.

3. Description of the steady free-stream separating turbulent boundary layer

The wind-tunnel geometry and the steady separated flow used here were the same as reported and discussed by Simpson *et al.* (1981). Figure 2 of that paper shows that the core inviscid velocity increases from 15 m s^{-1} at the test-section entrance to 21.8 m s^{-1} at 1.63 m. Downstream the pressure gradient is increasingly positive until 2.5 m, where the slope of the static pressure gradient changes sign. Near 3.7 m the pressure gradient drops to an approximately constant value until 5 m.

The detachment state at 1 mm from the wall for this flow can be described as follows (Simpson *et al.* 1981): incipient detachment (ID) occurs at 3.1 m with instantaneous backflow 1 % of the time; intermittent transitory detachment (ITD) occurs at 3.3 m with instantaneous backflow 20 % of the time; transitory detachment (TD) occurs at 3.45 m with instantaneous backflow 50 % of the time; and detachment (D) also occurs at 3.45 m where the time-averaged wall shearing stress $\bar{\tau}_w = 0$.

Downstream of detachment, high turbulence levels exist in the backflow, with u- and v-fluctuations of the same order as $|U|$. The fraction of time with forward flow γ_{pu} never reaches zero, indicating that there is no location with backflow all of the time. Either high-momentum forward flow moves toward the wall or high-momentum turbulent motions away from the wall set up instantaneous streamwise pressure gradients that are impressed onto the low-momentum wall region to produce instants of forward flow (Simpson 1985). Normal and shear-stress turbulence-energy production in the outer region supplies turbulence energy to the backflow by turbulence diffusion where it is dissipated. Negligible turbulence-energy production occurs in the backflow. The backflow does not come from far downstream. The frequency of passage n of these large-scale structures also varies as U_∞/δ and is about an order-of-magnitude smaller than the frequency far upstream of detachment. Reynolds shearing stresses in the backflow are related to the turbulence structure and not to local mean-velocity gradients. The mean-velocity profiles in the backflow are a result of time averaging of the large fluctuations and are not related to the cause of the turbulence.

Simpson, Ghodbane & McGrath (1984) report velocity spectra and wave speeds for this flow. The spectrum function $F(n) \sim n^{-1}$ near the wall upstream of detachment and $F(n) \sim n^{-\frac{5}{3}}$ in the higher-frequency inertial subrange. The wave speed or celerity increases at low frequencies to the local mean velocity at high frequencies, as observed by Strickland & Simpson (1973) for another separating turbulent boundary layer. The ratio of the wave speed U_c to the local mean velocity is given approximately by

$$\frac{U_c}{U} = \frac{2\pi nL}{2\pi nL + U},$$

where L is a lengthscale. L decreases with increasing streamwise position, reflecting the strong deceleration of the large-scale structures. At a given streamwise position, L increases to a maximum.

4. Instrumentation and experimental techniques

4.1. *Microphones and calibrations*

Two Sennheiser Model MKH-110 Instrumentation Microphones were each mounted in identical 2.21 cm diameter Plexiglas housings with 0.074 cm diameter ($dU_\tau/\nu < 43$) by 0.025 cm long pinholes in the flat end for use in these measurements. According to the manufacturer's specifications, these low-frequency RF condensor microphones have a nominal sensitivity of 20 mV/Pa, nearly flat frequency response (± 3 dB) between 1 Hz and 6 KHz, an overload level of 120 dB SPL, and signal-to-noise ratio of 63 dB $\pm$ 3 dB. The frequency response peaks at about 10 KHz and drops below the low-frequency level at 16 KHz. Each microphone was modified to produce equal static pressures on both sides of the diaphragm and was calibrated, as discussed by Simpson *et al.* (1984).

For coherence and celerity measurements when the two microphones are close together, two housings were joined adjacently. Several of the above-mentioned pinholes were located on each housing end, permitting sensing hole spacings of 1.40 to 3.02 cm. Pinholes not in use were covered by thin cellophane tape.

4.2. *Pressure-fluctuation measurement techniques*

After initial use of these microphones, it was apparent that minute wind-tunnel vibrations and acoustic disturbances make large contributions to the microphone signals. To eliminate the vibration effects, the microphones and housings were supported directly from the concrete flooring, with no direct firm contact with the adjacent test wall. Strips of 0.05 mm thick cellophane tape were used to make the test surface flat and continuous between the 3.5 cm diameter holes in the test wall and the Plexiglas housings.

In this wind tunnel, there are streamwise acoustic disturbances that propagate downstream from the blower-muffler-plenum-honeycomb-screen sections into the contraction. The contraction and test section, which are 0.92 m wide, act as wave guides for these disturbances, so that at any streamwise location the streamwise acoustic waves are the same across the test section at any instant in time. The turbulent-flow-produced spectrum is the same across the test section because the mean flow and mean-square turbulence structure are two-dimensional across the centre of the flow (Simpson, Chew & Shivaprasad 1980). The acoustic and turbulent signals are uncorrelated, since we can see from (2) and (3) that the turbulence-produced signal is due to the locally produced velocity field. These observations permit us to use two microphones in a novel way to decompose the surface

pressure-fluctuation signals into the propagated acoustic part and the turbulent-flow-generated portion.

The two microphones and housings are spaced far apart spanwise ΔZ across the test section so that the turbulent signals are uncorrelated. The minimum distance between sensors to produce a zero cross-correlation is about $\frac{1}{2}\delta$, where δ is the shear-layer thickness (Simpson *et al.* 1977). Physically this means that individual large-scaled motions are no more than about δ in spanwise extent and are unrelated to one another. In practice, for spectral measurements, ΔZ was 15 cm far upstream of detachment where $\delta < 6$ cm and 30 cm in the detached zone where $\delta < 30$ cm.

At any spectral frequency n, the time-dependent signals detected by these two microphones can be written as

$$p_{1n} = p_{1\mathrm{A}n} + p_{1\mathrm{T}n}, \tag{14a}$$

$$p_{2n} = p_{2\mathrm{A}n} + p_{2\mathrm{T}n}, \tag{14b}$$

where the subscripts A and T denote the acoustic and turbulent portions. If we *subtract* p_{2n} from p_{1n} and obtain the mean-square value of the result, then

$$\overline{p^2_{1\mathrm{T}n}} = \tfrac{1}{2}\overline{(p_{1n} - p_{2n})^2} \tag{15}$$

is the turbulent spectral contribution at frequency n because

$$\overline{p^2_{1\mathrm{T}n}} = \overline{p^2_{2\mathrm{T}n}} \quad \text{(mean two-dimensional flow)}, \tag{16a}$$

$$\overline{p_{1\mathrm{T}n}\, p_{2\mathrm{T}n}} = 0 \quad \text{(uncorrelated turbulent contributions)}, \tag{16b}$$

$$p_{1\mathrm{A}n} = P_{2\mathrm{A}n} \quad \text{(same acoustic signals)}. \tag{16c}$$

Under these conditions and the condition

$$\overline{p_{1\mathrm{A}n}\, p_{1\mathrm{T}n}} = \overline{p_{2\mathrm{A}n}\, p_{2\mathrm{T}n}} = \overline{p_{1\mathrm{A}n}\, p_{2\mathrm{T}n}} = \overline{p_{2\mathrm{A}n}\, p_{1\mathrm{T}n}} = 0 \tag{16d}$$

(uncorrelated acoustic and turbulent contributions)

the acoustic contribution at frequency n is given by

$$\overline{p^2_{1\mathrm{A}n}} = \tfrac{1}{4}\overline{(p_{1n} + p_{2n})^2} - \tfrac{1}{2}\overline{p^2_{1\mathrm{T}n}}. \tag{17}$$

The two microphones are located equidistantly about the tunnel centreline. Thus, (15) provides the proper turbulent spectrum for frequencies below c/w, where c is the speed of sound and w is the contraction and test section width (370 Hz). In other words, longitudinal, vertical and spanwise acoustic contributions that are the same at the two microphones are eliminated. However, spanwise acoustic contributions near frequency c/w and higher harmonics are added because of the antisymmetry of that mode. For those frequencies the turbulent contribution must be obtained by

$$p^2_{1\mathrm{T}n} = \tfrac{1}{2}\overline{(p_{1n} + p_{2n})^2} \tag{18}$$

so that the acoustic contributions cancel. An experimental-uncertainty analysis shows a negligible uncertainty in the resulting turbulent spectrum obtained in this manner when the sensitivities of the two microphones are matched, as discussed in §4.3 below.

To determine the convective wave speed of the turbulent contributions, the two microphones were spaced a small distance ΔX apart in the streamwise direction. The wave speed or celerity at frequency n is given by

$$U_{\mathrm{c}} = \frac{\omega \Delta X}{\phi_{tn}}, \tag{19}$$

where
$$\tan \phi_{tn} = I_{tn}/R_{tn}, \tag{20}$$

$$\gamma^2(\Delta X, n) = R_{tn}^2 + I_{tn}^2. \tag{21}$$

Here γ^2 is the coherence and R_{tn} and I_{tn} are the normalized real and imaginary parts of the cross-spectral density of the turbulent contributions (Bendat & Piersol 1971). Because the acoustic contributions at the two different streamwise locations are coherent but time delayed, they can be accounted for using the measured acoustic spectra. In other words, since

$$p_{2An} = p_{1An}\, e^{-i\omega \Delta X/C} \tag{22}$$

we can use (15) in the streamwise direction to calculate only the turbulent contributions to R_{tn} and I_{tn}. The acoustic contributions tend to cancel. In practice the acoustic contributions were less than 10 % of other terms due to the turbulence.

4.3. *Signal processing*

For the pressure spectra and celerity data, the signals from each of the microphones were input to a TSI Model 1015C Correlator where the effective V/Pa sensitivities were equalized very closely with slightly different amplification ratios. Thus, with closely equal effective sensitivities, it is possible to use the sum or difference of these signals to determine pressure spectral and celerity information, as discussed in §4.2 above.

The sum or difference of these two instantaneous signals was input to a Princeton Applied Research (PAR) Model 4512 fast-Fourier-transform spectrum analyzer. The frequency resolution is 1/512 of the selectable frequency range of this 512 bin digital unit. Data records were at least 2 minutes long, which was experimentally verified to be sufficiently long for closely repeatable spectral results.

The logarithm of the content of each bin of a spectrum was transferred from the PAR to an HP 9825T digital computer for storage and further processing. Use of the logarithms of the data preserved a 1 bit uncertainty of the spectral results for the final processing. Mean-square fluctuation values were computed by summing the square of the antilogarithm values for each bin, taking into account the proper transfer function and calibration values.

5. Experimental results

5.1. *Surface pressure-fluctuation spectra*

Figures 2 and 3 show surface pressure-fluctuation spectra $\Phi(\omega)$ for the adverse-pressure-gradient region upstream of incipient detachment (ID) at 3.11 m where there is no intermittent backflow near the wall. As documented by Simpson *et al.* (1981) for this flow, the wall shear stress decreases along the flow while the maximum shear stress decreases slightly. Figures 4 and 5 show surface pressure-fluctuation spectra downstream of the beginning of intermittent backflow. The maximum shear stress increases while the mean wall shear stress decreases to zero at detachment at 3.52 m, and is negative downstream. As shown in table 2, τ_M/τ_w and $\overline{p^2}$ increase along the flow.

The results in figures 2–5 have no more than ± 1 dB uncertainty. For frequencies below 15 Hz, $\Phi(\omega)$ is about constant upstream of detachment. For higher frequencies less than 150 Hz, $\omega\Phi(\omega)$ is about constant upstream of incipient detachment. The acoustic spectra for this wind tunnel, obtained by (17), are about 10 dB higher than

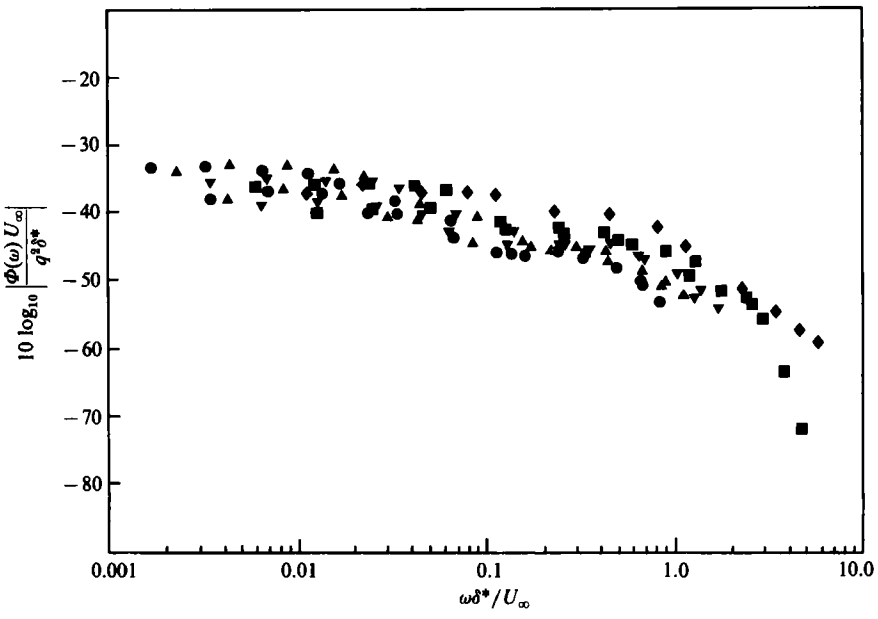

FIGURE 2. Surface pressure spectra upstream of incipient detachment, normalized on local free-stream dynamic pressure q, δ^*, and U_∞: ●, $X = 1.63$ m; ▲, 1.89 m; ▼, 2.22 m; ■, 2.54 m; ◆, 2.85 m.

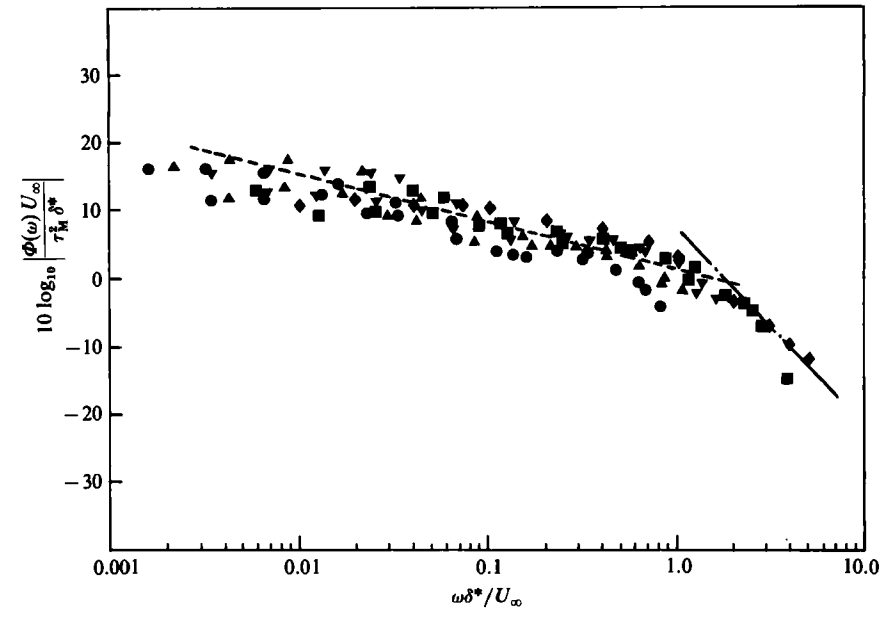

FIGURE 3. Surface pressure spectra upstream of incipient detachment, normalized on local τ_M, δ_1, and U_∞. – – –, $\omega^{-0.7}$ variation; —·—·—, ω^{-3} variation. For symbols see figure 2.

turbulent spectra and contain many discrete spectral peaks, unlike the smooth turbulent spectra shown in figures 2–5.

For these locations there is about a 3 dB hump in each $\omega\Phi(\omega)$-spectrum around 500 Hz. At first glance this is apparently the pinhole-related amplification of a certain frequency range described by Bull & Thomas and discussed in §2. This effect does

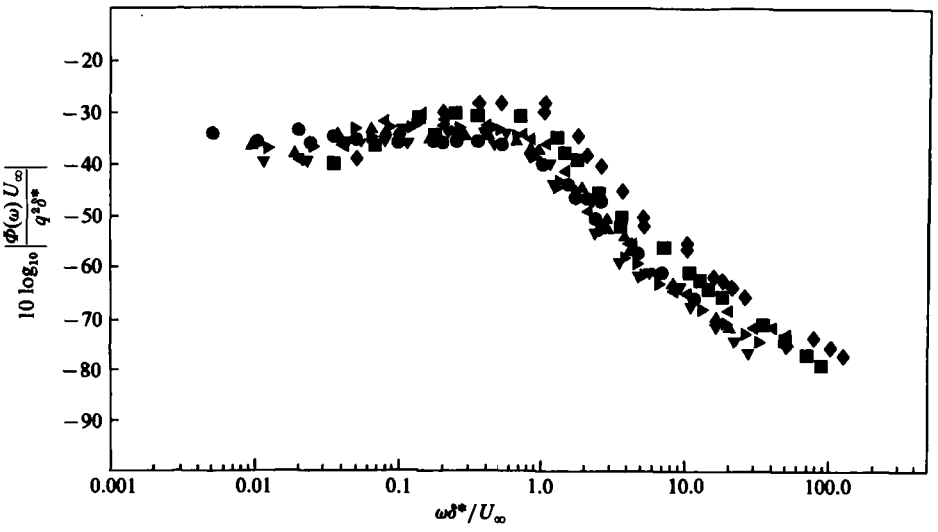

FIGURE 4. Surface pressure spectra downstream of incipient detachment normalized on q, δ^*, and U_∞. X = ●, 3.11 m; ▲, 3.28 m; ▼, 3.42 m; ▶, 3.53 m; ◀, 3.75 △: ■, 4.14 m; ◆, 4.42 m.

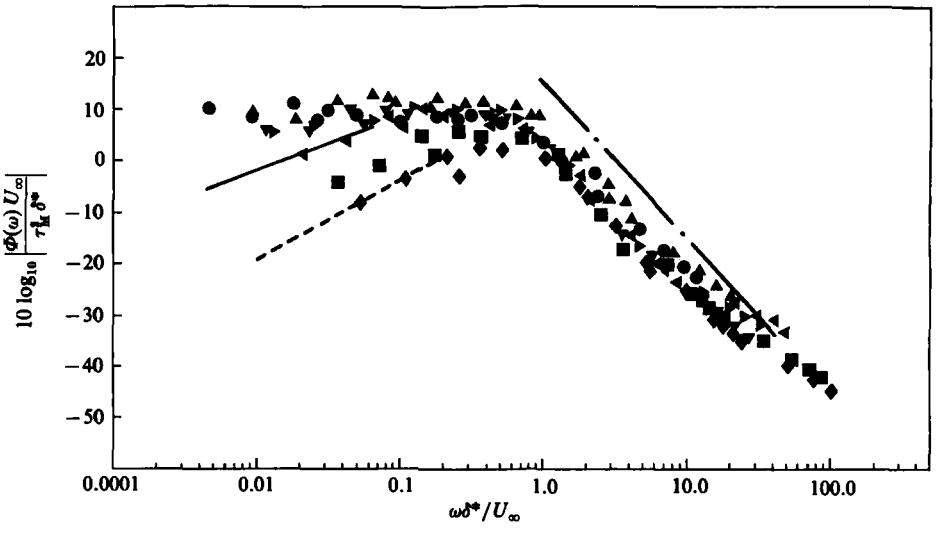

FIGURE 5. Surface pressure spectra downstream of incipient detachment, normalized on τ_M. ——, ω-variation; – – – –, $\omega^{1.4}$ variation; —·—, ω^{-3} variation. For symbols see figure 4.

not cancel when subtracting the signal from two equally sensitive microphones when using (15). Bull & Thomas only examined zero-pressure-gradient cases and concluded that $\omega\nu/U_\tau^2 > 0.1$ for this effect to be important. On this criterion, $\omega\nu/U_\tau^2 < 0.1$ for the present data under 1 KHz upstream of incipient detachment, making this pinhole effect appear to be unrelated to the humps in the $\omega\Phi(\omega)$-spectra near 500 Hz.

If we re-examine the Bull & Thomas data, we see that the wavelengths that were amplified in their experiments are equal to the pinhole diameter when $1 < \omega\nu/U_\tau^2 < 2$. In other words, when $nd/U_c \approx 1$, spurious amplification of pressure fluctuations occurred for the Bull & Thomas pinhole data. The present data produce values of $nd/U_c < 0.1$ for the observed humps. Thus, it is reasonable to conclude that the Bull

X location (m)	U_∞ (m s^{-1})	δ^* (cm)	$\frac{U_M}{U_\infty}$	$\frac{\tau_M}{\tau_w}$	$\overline{p^2}$ (Pa^2)	$\frac{\overline{p^2}}{\tau_M^2}$	$\frac{p'}{\tau_M}\left(\frac{NU_M}{N_d U_\infty}\right)^{\frac{1}{4}}$	N (cm)	$10\log_{10}\left(\frac{\Phi(\omega)U_\infty}{\delta^*\tau_M^2}\right)$ at $\omega\delta^*/U_\infty = \frac{1}{2}$
1.63	21.8	0.28	0.042	1.0	5.00	5.29	—	—	2.01
1.89	21.3	0.38	0.040	1.04	5.45	7.65	—	—	2.31
2.22	20.4	0.55	0.038	1.08	5.87	11.7	—	0.38	3.11
2.54	18.8	0.96	0.042	1.77	6.60	11.7	—	0.81	4.11
2.85	17.0	1.60	0.046	3.08	8.87	16.2	—	1.68	5.51
3.11	15.1	3.05	0.055	—	10.7	15.3	—	4.1	8.01
3.28	14.4	5.08	0.050	—	11.8	31.0	2.32	4.7	11.01
3.42	14.3	6.78	0.058	—	12.0	17.7	1.68	7.4	8.01
3.53	14.0	7.90	0.060	—	12.7	19.0	1.70	6.8	8.01
3.75	13.6	11.6	0.068	—	14.4	14.1	1.78	10.7	9.01
4.14	12.5	18.3	0.078	—	17.3	7.02	1.52	16.5	4.01
4.42	10.7	22.2	0.121	—	17.2	4.41	1.50	20.5	2.01

TABLE 2. Experimental data presented here for the Simpson *et al.* (1981) separating turbulent boundary layer

& Thomas pinhole effect is unimportant for these data and that the observed humps are produced by the turbulent flow. If one compares these spectra with the velocity spectra (Simpson *et al.* 1984), it appears that the low-frequency end of each hump coincides closely with the low-frequency end of the $n^{-\frac{2}{3}}$ region for the $nF(n)$ velocity spectra.

Figures 2 and 3 show the spectral data for the attached flow in non-dimensional coordinates. The Corcos (1963) sensor-resolution correction was applied to these data and amounted to the order of 1 dB at the higher frequencies. The free-stream dynamic pressure has less direct influence on the pressure spectra than the local streamwise maximum shearing stress τ_M. Consequently, figure 3 shows a slightly tighter correlation of the ordinate values than shown in figure 2 in terms of the dynamic pressure.

Figure 3 shows that for $\omega\delta^*/U_\infty < 1$, the spectra vary approximately like $\omega^{-0.7}$, which is observed in the data of Brooks & Hodgson (1981) for a NACA 0012 airfoil and was observed by McGrath & Simpson (1985) for zero- and favourable-pressure-gradient flows with $Re_\theta < 5000$. In the strong adverse-pressure-gradient region, $\phi(\omega) \sim \omega^{-3}$ at the higher frequencies. None of the data shown in figure 1 extend below $\omega\delta^*/U_\infty = 0.1$, so the present data define the low-frequency region. The Panton & Linebarger theory does not agree with the frequency variation of the present data for $\omega\delta^*/U_\infty < 0.3$.

Figures 4 and 5 show the surface pressure spectra downstream of incipient detachment in non-dimensional coordinates. In figure 4 $\Phi(\omega)$ is normalized on q; this plot masks the true variations at low frequencies that are observed in figure 5 and a $\omega\Phi(\omega)$-plot. Figure 5 shows that normalization on τ_M produces a much tighter correlation for $\omega\delta^*/U_\infty > 1$. The Corcos (1963) microphone-resolution correction was not applied to these data because large-wavelength motions dominate the detached flow and require negligible correction. Furthermore, and more importantly, the instantaneous flow reversal contains small and large wavelength motions that as yet cannot be related to specific frequencies.

Figure 5 clearly shows the ω^{-3} dependence of $\Phi(\omega)$ at the higher frequencies of the detaching flow. This ω^{-3} behaviour has been observed in the data of Kiya *et al.* (1982)

for a separated forward-facing step flow, and Bradshaw (1967), Burton (1973) and Schloemer (1967) for adverse-pressure-gradient boundary layers. When we compare figure 3 and table 2 with figure 1, we see that $\Phi(\omega)$ has appoximately the same shape and magnitude as for the earlier attached-flow investigations.

Figure 5 shows that the frequency range where $\Phi(\omega)$ is constant decreases continuously in the downstream direction. At the lowest frequencies downstream of detachment, $\Phi(\omega)$ varies with ω to a power greater than one. Figure 5 shows that the peak frequency of $\omega\Phi(\omega)$ and the ω^{-3} high-frequency range of the spectra in figure 5 can be correlated using this non-dimensional frequency $\omega\delta^*/U_\infty$. The peak occurs at $\omega\delta^*/U_\infty \approx 0.8$ and the ω^{-3} range extends to about 6. The peak frequencies of $nF(n)$ for the streamwise velocity spectra near the maximum-shearing-stress location ($y/\delta \approx 0.5$) are approximately the same as peak frequencies for $\omega\Phi(\omega)$. The streamwise velocity spectra in the intermittent backflow region obtained by Simpson *et al.* (1981) with a laser anemometer indicate that $nF(n)$ is constant for $0.07 < \omega\delta^*/U_\infty < 0.5$, which is below the peak frequency of $\omega\Phi(\omega)$.

Figure 6 shows the r.m.s. pressure values p' computed from these data and normalized on the reference inlet dynamic pressure q_{ref}, the local wall shear stress τ_{w}, and the local maximum shear stress τ_{M}. The uncertainty in p' is about $\pm 20\%$. Although p' increases along the flow, p'/τ_{M} increases to detachment and then decreases. At $X = 1.63$ m at the end of the favourable-pressure-gradient region, $p'/\tau_{\text{w}} = 2.3$, which is in good agreement with values obtained by McGrath & Simpson (1985) for a favourable-pressure-gradient flow at the same Re_θ but with different pinhole microphones.

5.2. *Surface pressure-fluctuation celerities*

Figures 7 and 8 show the square root of the coherence for two microphones whose pinholes are separated by ΔX in the streamwise direction. These results were obtained using (19)–(22) and have an uncertainty of ± 0.05. The values of γ are low, indicating a large decay in similarity of the pressure signals between microphones. Like the data of Brooks & Hodgson (1981) and of Hahn (1976), γ increases with frequency to a maximum in the frequency range where $\omega\Phi(\omega)$ is a maximum for the locations upstream of incipient detachment. At higher frequencies γ drops to very low values.

Corcos (1963) proposed that the cross-spectrum in the lateral and longitudinal directions decays exponentially with the phase angle ϕ. In terms of the square root of the coherence

$$\gamma = \exp\left(-K_1\phi - K_3\left(\frac{\Delta Z}{\Delta X}\right)\phi\right). \tag{23}$$

Upstream of incipient detachment $K_1 = 0.12$, as shown in figure 7. At the lower values of ϕ, agreement with (23) is poor, but Brooks & Hodgson found a similar behaviour. This value of K_1 seems low for a strong adverse-pressure-gradient flow in view of Schloemer's (1967) result that K_1 is greater for adverse pressure gradients than for zero pressure gradients. Zero-pressure-gradient values of 0.11 to 0.23 have been reported (Corcos 1963; McGrath & Simpson 1985; Brooks & Hodgson 1981).

After some intermittent backflow begins downstream of incipient detachment, the value of K_1 appears to drastically increase, as shown in figures 7 and 8. $K_1 = 0.75$ approximately describes the data at $X = 3.28$ m and 3.53 m; $K_1 \approx 1.0$ at $X = 4.14$ m. These values of K_1 are close to the values of K_3 near 0.75 reported for the lateral or spanwise decay of γ for zero-and adverse-pressure-gradient attached boundary layers (Corcos 1963; McGrath & Simpson 1985; Brooks & Hodgson 1981;

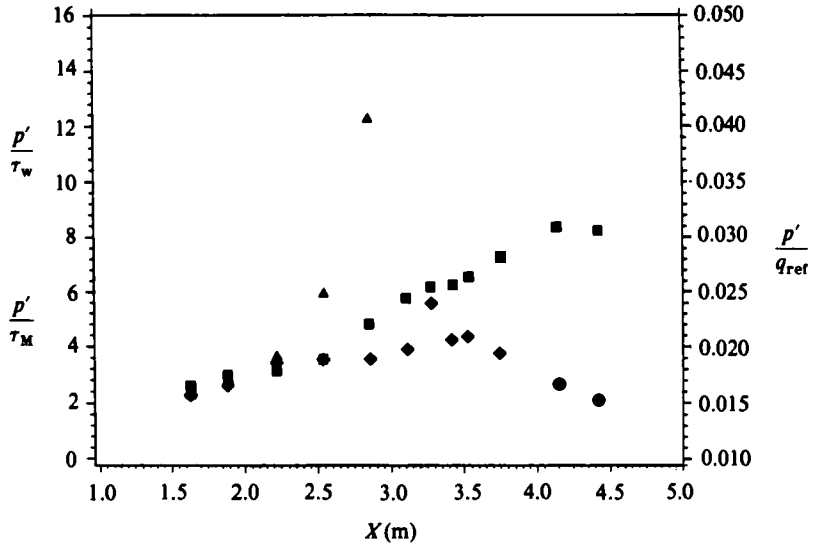

FIGURE 6. Streamwise distribution of p'/q_{ref} (■), p'/τ_w (▲), and p'/τ_M (◆).

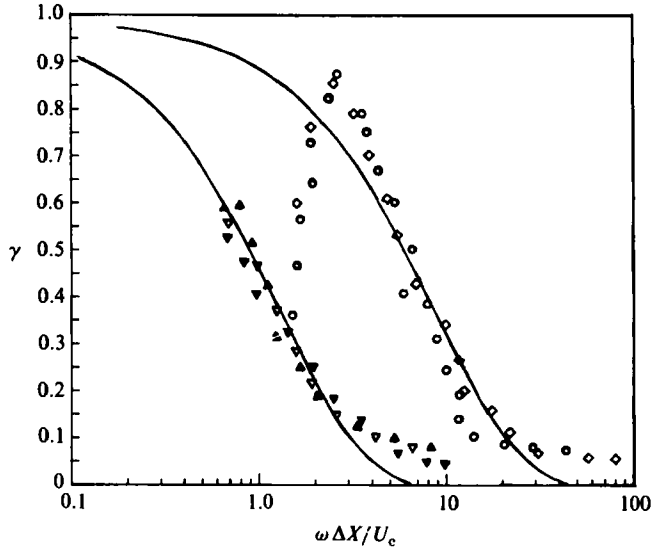

FIGURE 7. Square root of streamwise coherence upstream of and in the detachment zone. Upper line: $K_1 = 0.12$ in (26); lower line: $K_1 = 0.75$ in (26): ○, $X = 2.22$ m, $\Delta X/\delta^* = 2.55$; ◇, 2.85 m, $\Delta X/\delta^* = 0.28$; ▽, 3.28 m, $\Delta X/\delta^* = 0.28$; ▲, 3.28 m; $\Delta X/\delta^* = 0.44$; ▼, 3.28 m; $\Delta X/\delta^* = 0.60$.

Blake 1970; Burton 1973). This suggests, as do the flow-field data, that the intermittent backflow destroys the streamwise coherence of pressure fluctuations.

Figure 9 shows that upstream of incipient detachment, U_c increases with increasing frequency till near $\omega\delta^*/U_\infty = 1$ as observed by Brooks & Hodgson. U_c decreases at higher frequencies and agrees asymptotically with (13) for the inner–outer overlap region. After the beginning of intermittent backflow, U_c no longer agrees with (13) and very low values of U_c are observed. These data are from all of the close ΔX spacings given in figures 7 and 8; there is no apparent effect of spacing. The experimental uncertainty for U_c/U_e is about ± 0.05.

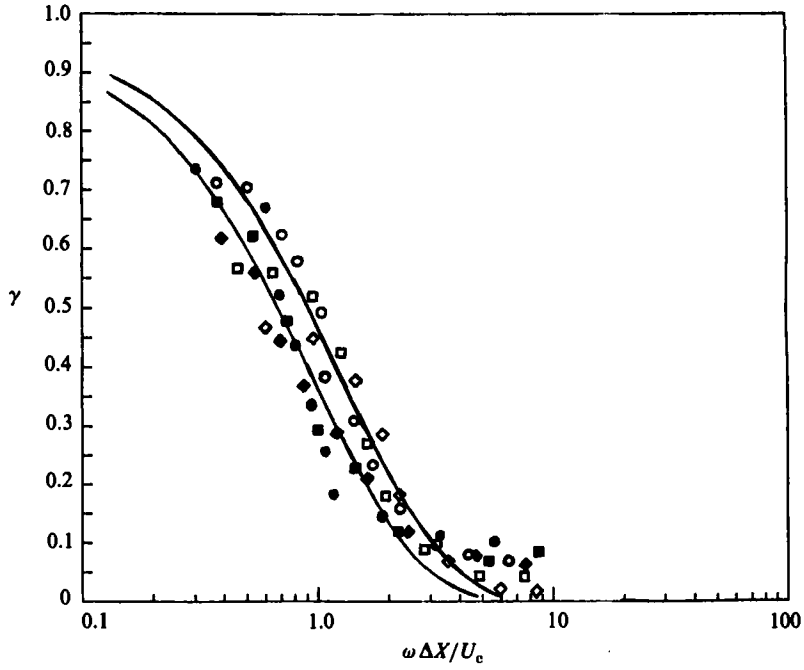

FIGURE 8. Square root of streamwise coherence downstream of detachment. Top line, (26) with $K_1 = 0.75$; bottom line, (26) with $K_1 = 1.00$. At 3.53 m: ○, $\Delta X/\delta^* = 0.177$; □, 0.283; ◇, 0.383. At 4.14 m: ●, $\Delta X/\delta^* = 0.076$; ■, 0.122; ◆, 0.165.

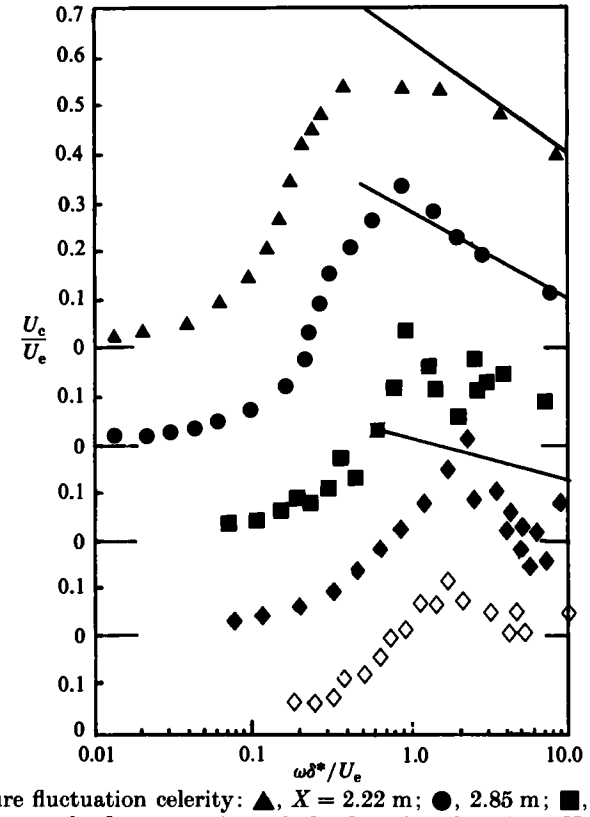

FIGURE 9. Pressure fluctuation celerity: ▲, $X = 2.22$ m; ●, 2.85 m; ■, 3.28 m; ◆, 3.53 m; ◇, 4.14 m. Solid lines: results from equation (13) for first three locations. Note displaced ordinates.

6. Discussion, summary and conclusions

Measurements of surface pressure-fluctuation spectra, r.m.s. values, wave speeds, and coherence have been reported for a nominally two-dimensional separating turbulent boundary layer. To our knowledge there are no other measurements available on these properties for such a separating turbulent boundary layer.

At the end of the favourable-pressure-gradient region far upstream of incipient detachment, $p'/\tau_w = 2.3$, which is in good agreement with values obtained by McGrath & Simpson (1985) for a favourable-pressure-gradient flow at the same Re_θ. The ratio $\overline{p^2}/\tau_M^2$ is substantially larger for the attached strong adverse-pressure-gradient part of the present flow than in the investigations listed in table 1. As discussed in §2, $\overline{p^2}/\tau_M^2$ is proportional to the ratio of streamwise lengthscale to lengthscales in other directions α. The integral-lengthscale data of Chehroudi & Simpson (1985) show that α is about 2.5 for this flow, which is in agreement with the Schubauer & Klebanoff (1951) results for α in their separating flow. Thus, the present results for $\overline{p^2}/\tau_M^2$ upstream of detachment appear plausible. This apparent importance of α on $\overline{p^2}$ suggests that space–time velocity correlations should be obtained in future experiments to determine integral lengthscales.

Downstream of detachment, $\overline{p^2}$ continues to increase, although p'/q_{ref} does not reach the values of 0.04 to 0.1 that were observed by Mabey (1972) for step-induced separation and reattachment flows. The ratio p'/τ_M increases to detachment and then decreases downstream. The level of p'/τ_M for these data seems reasonable since Kiya *et al.* (1982) observed values of $p'/\tau_M \approx 10$ for a forward-facing step flow. This decrease appears to be because the pressure-fluctuation-producing motions move increasingly away from the wall downstream of detachment.

Both the turbulence and mean-shear interaction and the turbulence–turbulence interaction in the pressure-fluctuation source term, (2), are important for detached flows. Velocity fluctuations are as large as mean velocities in the backflow. Reynolds shear stresses and their gradients are large away from the wall. Thus the largest pressure fluctuations are not at the wall in a detached flow, but must be near the middle of the shear layer. Equation (3) indicates that $p(\boldsymbol{x})$ on the wall must decrease if the source σ moves away from the wall. Table 2 shows that the distance from the wall to the maximum shear location N increases rapidly downstream of detachment.

In order to try to correlate this effect, a modified version of (12) was used. First, N/δ^* is almost constant downstream of detachment and $(U_\infty/U_M)^{\frac{1}{3}}$ does not vary enough to correlate p'/τ_M. As shown in table 2,

$$\frac{p'}{\tau_M}\left(\frac{NU_M}{N_d U_\infty}\right)^{\frac{1}{3}} \approx 1.64 \pm 8\,\%, \tag{24}$$

where N_d is the distance of the maximum shear stress location from the wall at detachment.

The spectra for $\overline{p^2}$ substantially agree with those of other investigations of strong adverse-pressure-gradient attached flows, which were reanalysed and renormalized on τ_M. The present data define a $\omega^{-0.7}$ variation in the $0.01 < \omega\delta^*/U_\infty < 1$ range for the attached flow. At higher frequencies $\Phi(\omega)$ varies with ω^{-3}. Downstream of the beginning of intermittent backflow, $\omega\Phi(\omega)$ has a peak near $\omega\delta^*/U_\infty \approx 0.8$ and a ω^{-2} range at higher frequencies. For lower frequencies, $\omega\Phi(\omega)$ varies with ω near the beginning of intermittent backflow; farther downstream this low-frequency range varies with $\omega^{2.4}$.

The coherence of the pressure-fluctuation-producing motions remains high in the

streamwise direction upstream of incipient detachment but drops drastically with the beginning of intermittent backflow. The streamwise coherence level downstream of detachment looks much like that for the spanwise direction for attached flows. This indicates that even over small streamwise distances, the detached-flow pressure-fluctuation-producing turbulent motions do not retain the same structural features.

At low frequencies, both upstream and downstream of detachment, U_c celerity results are reasonable and agree qualitatively with other available data. Upstream of detachment at high frequencies the data agree asymptotically with the overlap region celerity, (13). The relatively large size of the two microphones used in this work prevented celerity measurements at closer spacings. Downstream of the beginning of intermittent backflow, the instantaneous wave speed U_c can be both positive and negative for sufficiently high frequencies. Thus, the long-time-averaged U_c is lower than at upstream for these frequencies.

From the perspective of using pressure-fluctuation data to calculate far-field noise, one should probably locate the effective pressure-fluctuation sources along or near the locus of the maximum shear stress position. The pressure-fluctuation-producing motions are concentrated in this region. The celerities of these fluid motions are probably close to those for the pressure fluctuations in this region.

This hypothesis is consistent with the idea of placing the effective pressure-fluctuation sources on the flow surface for low-pressure-gradient flows, since in these cases the maximum velocity gradients and shear stresses are at or very close to the wall. Since it is not possible to accurately measure pressure fluctuations within the turbulent separated flow, measurements of the far-field pressure fluctuation and the wall pressure fluctuation should be used to estimate the effective pressure fluctuations at the maximum-shearing-stress location.

This work was supported by the National Aeronautics and Space Administration, Langley Research Center, under Grant NAG-317 monitored by Dr Thomas F. Brooks.

REFERENCES

BENDAT, J. S. & PIERSOL, A. G. 1971 *Random Data: Analysis and Measurement Procedures.* Wiley-Interscience.

BLAKE, W. K. 1970 *J. Fluid Mech.* **44**, 637–660.

BRADSHAW, P. 1967 *J. Fluid Mech.* **30**, 241–258.

BROOKS, T. F. & HODGSON, T. H. 1981 *J. Sound Vib.* **78**, 69–117.

BROOKS, T. F. & SCHLINKER, R. H. 1983 *Vertica* **7**, 287–307.

BULL, M. K. 1967 *J. Fluid Mech.* **28**, 719–754.

BULL, M. K. & THOMAS, A. S. W. 1976 *Phys. Fluids* **19**, 597–599.

BURTON, T. E. 1973 *Acoustics and Vibration Lab. MIT. Rep.* 70208–9.

CHEHROUDI, B. & SIMPSON, R. L. 1985 *J. Fluid Mech.* **160**, 77–92.

COLES, D. E. & HIRST, E. (eds) 1969 *Computation of Turbulent Boundary Layers – 1968 AFOSR-IFP-Stanford Conference*, Stanford University, Department of Mechanical Engineering.

CORCOS, G. M. 1963 *J. Acoust. Soc. Am.* **35**, 192–199.

EAST, L. F. & SAWYER, W. G. 1979 *AGARD CP*-271, paper 6.

HAHN, M. 1976 *AIAA paper* 76-335.

KIYA, A., SASAKI, K. & ARIE, M. 1982 *J. Fluid Mech.* **120**, 219–244.

LIM, K. G. 1971 Ph.D. thesis, Department of Mechanical Engineering, University of Adelaide.

MABEY, D. G. 1972 *J. Aircraft* **9**, 642–645.

MABEY, D. G. 1982 *AIAA J.* **20**, 1632.

McGrath, B. E. & Simpson, R. L. 1985 *NASA CR Rep.* (in press); M.S. thesis, Dept. Aero. and Ocean Engrg., Virginia Polytechnic Institute and State University.

Panton, R. L. & Linebarger, H. G. 1974 *J. Fluid Mech.* **65**, 261–287.

Perry, A. E. & Schofield, W. H. 1973 *Phys. Fluids* **16**, 2068–2074.

Schloemer, H. H. 1967 *J. Acoust. Soc. Am.* **42**, 93–113.

Schubauer, G. B. & Klebanoff, P. S. 1951 *NACA Rep.* 1030.

Simpson, R. L. 1976 *Max-Planck-Institut für Strömungsforschung Bericht* 118.

Simpson, R. L. 1981 *Trans. ASME* I: *J. Fluids Engng* **103**, 520–533.

Simpson, R. L. 1985 *AGARDograph* 287, vol. 1, p. 21.

Simpson, R. L., Chew, Y.-T. & Shivaprasad, B. G. 1980 *Project SQUID Rep.* SMU-4-PU; NTIS AD-A095 252/3.

Simpson, R. L., Ghodbane, M. & McGrath, B. E. 1984 An experimental study of surface pressure fluctuations in a separating turbulent boundary layer. *NASA CR Rep.* (in press).

Simpson, R. L., Shivaprasad, B. G. & Chew, Y.-T. 1981 *J. Fluid Mech.* **113**, 23–74.

Simpson, R. L., Strickland, J. H. & Barr, P. W. 1977 *J. Fluid Mech.* **79**, 553–594.

Strickland, J. H. & Simpson, R. L. 1973 *Thermal and Fluid Sciences Center Rep.* WT-2, also AD-771170/8GA. Southern Methodist University.

Willmarth, W. W. 1975 *Ann. Rev. Fluid Mech.* **7**, 13–38.

Wills, J. A. B. 1970 *J. Fluid Mech.* **45**, 65–90.